HAL
open science

Zeolite-Reinforced Interpenetrating Polymer Network Initiated by Chalcone Based Photoinitiating System and Their Application in 3D/4D Printing

Yijun Zhang, Hong Chen, Loïc Vidal, Gautier Schrodj, Fabrice Morlet-Savary, Frédéric Dumur, Angélique Simon-Masseron, Jacques Lalevée

To cite this version:

Yijun Zhang, Hong Chen, Loïc Vidal, Gautier Schrodj, Fabrice Morlet-Savary, et al.. Zeolite-Reinforced Interpenetrating Polymer Network Initiated by Chalcone Based Photoinitiating System and Their Application in 3D/4D Printing. Advanced Materials Technologies, In press, 10.1002/admt.202200074 . hal-03712517

HAL Id: hal-03712517

https://hal.science/hal-03712517v1

Submitted on 4 Jul 2022

HAL is a multi-disciplinary open access archive for the deposit and dissemination of scientific research documents, whether they are published or not. The documents may come from teaching and research institutions in France or abroad, or from public or private research centers.

L'archive ouverte pluridisciplinaire **HAL**, est destinée au dépôt et à la diffusion de documents scientifiques de niveau recherche, publiés ou non, émanant des établissements d'enseignement et de recherche français ou étrangers, des laboratoires publics ou privés.

Zeolite-Reinforced Interpenetrating Polymer Network Initiated by Chalcone Based Photoinitiating System and Their Application in 3D/4D Printing

Yijun Zhang [1,2], Hong Chen [1,2], Loïc Vidal [1,2], Gautier Schrodj [1,2], Fabrice Morlet-Savary [1,2], Frédéric Dumur [3*], Angélique Simon-Masseron [1,2*], and Jacques Lalevée [1,2*]

[1] Université de Haute-Alsace, CNRS, IS2M UMR 7361, F-68100 Mulhouse, France

[2] Université de Strasbourg, France

[3] Aix Marseille Univ, CNRS, ICR, UMR 7273, F-13397 Marseille, France

* Corresponding authors:

Jacques Lalevée, jacques.lalevee@uha.fr

Angélique Simon-Masseron, angelique.simon-masseron@uha.fr

Frédéric Dumur, frederic.dumur@univ-amu.fr

Abstract

With the rapid development of photopolymerization, the search for new near-UV/visible light sensitive photoinitiating system (PIS) is the subject of intense research efforts. In this work, a new PIS (chalcone dye/amine/iodonium salt) could efficiently and simultaneously initiate the free radical photopolymerization (FRP) of PEGDA and the cationic photopolymerization (CP) of EPOX under irradiation of LED@405 nm to obtain interpenetrating polymer networks (IPNs). Then, the study on the photoinitiating abilities of the chalcone dye was examined to explain the chemical mechanisms through UV-visible absorption spectra, cyclic voltammetry, fluorescence approaches and electron spin resonance (ESR) spin-trapping experiments. Markedly, Chalcone is a class of natural dyes of flavonoids with potential low toxicity. Furthermore, this PIS was employed in the photopolymerization of LTA-5A zeolite filled interpenetrating polymer network composites (IPN, PEGDA/EPOX). Compared to the pure IPN, the depth of cure (DOC) for IPN with 50 wt% LTA-5A remarkably increased by ca. 90%, which was the first time reported that DOC could increase with the increase of the filler content. Compared to the storage modulus, tensile strength and Young's modulus of pure IPN, those of the IPN-composites containing 50 wt% LTA-5A increased by ca. 445 %, ca. 430 %, and ca.

580 %, respectively. By direct laser write (DLW), 3D patterns could be manufactured and those with high filler contents showed good water swelling property. Under hydrothermal stimuli, IPN composite with 50 wt% LTA-5A exhibited a good 4D printing behavior. Therefore, not only this chalcone dye has a good photoinitiation ability for photopolymerization, but also the resulting IPN composites prepared with the photoinitiating system containing this dye have potential applications for 3D/4D printing and composites preparation.

1. Introduction

Additive manufacturing (AM), also referred to as 3D printing, was first described in the 80's by Charles Hull, and this technique has evolved rapidly due to the ability to manufacture objects with complex spatial resolution.[1] Therefore, it has been applied in many fields, such as biomedical engineering,[2, 3] environmental protection,[4, 5] aerospace industries,[6] etc. 4D printing is also a very important application of 3D printing, with the addition of time as the fourth dimension.[7-9] The structure, color, function or other properties of 3D objects can be changed over time under the stimulus going from electricity to light, water, temperature, etc.[1, 10, 11] Due to these different stimuli, 4D printing will be used for grippers, smart textile, smart design, biomimetic materials and biomedical application.[12-14]

Normally, photopolymerization is a process enabling to transform a liquid monomer/oligomer into a solid polymer by use of a photoinitiating system (PIS) and upon irradiation with light (e.g. UV-light, visible light, sunlight, etc).[15-18] Compared to thermal polymerization, photopolymerization possesses many unique advantages, such as a high reaction rate, mild reaction temperature (normally room temperature), absence of organic solvents as volatile compounds (VOCs), low energy consumption, low-cost and safe optical source (LED), and enabling to get an excellent spatial and temporal control, etc.[18-20] Therefore, photopolymerization has been widely used in academia and industry.[21, 22] For photopolymerization, it always consists of a photoinitiating system (PIS), a polymerizable medium (M) and a light source (S), and these three parts are all necessary to get a polymerization.[20] Once the monomer/oligomer formulation is selected, the PIS, M and S will be strongly combined together to obtain the targeted polymers in the most efficient way.[1]

Now, there are a large amount of photoinitiators reported in the literature for photopolymerization. However, many of them are only adapted for UV irradiation and cannot even be activated in the near UV and the visible region, such as benzoin for Type I cleavage photoinitiator, and benzophenone for Type II H-abstraction photoinitiator.[23] Hence, it is meaningful to develop new high-performance photoinitiating system (PIS) with good photoinitiation ability under irradiation from near UV or visible region. [16, 19, 24-26] Recently, an extensive work has been devoted to develop new photoinitiating systems (PIS) of photopolymerization.[17, 27-32] Among all photoinitiators, natural photoinitiators are candidate of choice for the manufacture of biocompatible polymer materials.[33] Chalcone is a class of natural dyes belonging to the flavonoids and exhibiting a low toxicity. Chalcones can be found in many natural plants, such as fruits (apples, citrus), vegetables (shallots, bean sprouts and potatoes) and nuts.[34] Chalcones can exhibit different light absorption properties and color depending on the substituent as well as their positions onto the chalcone backbone. In the previous works of our group, over than 50 types of mono-chalcone derivatives have been studied as photoinitiators, due to their unique light absorption properties in the near UV or the visible range.[33-37] Interestingly, several mono-chalcone derivatives have exhibited good photoinitiation abilities for both free radical polymerization (FRP) of acrylates and the cationic photopolymerization (CP).[36] To further improve their performances, it is very necessary to find and synthesize novel chalcone derivatives in order to explore their photoinitiation abilities and get a deeper insight into the chemical mechanisms supporting the photopolymerization process.

Although 3D printing through photopolymerization can manufacture different 3D objects of pure polymer, the lack of mechanical properties and functions always limit the future development of 3D printing through photopolymerization.[1, 38] Hence, many types of fillers have been introduced into polymers to enhance/improve their mechanical properties and functions, such as alumina (Al_2O_3),[39, 40] zirconia (ZrO_2),[41] zeolites (LTA-5A, FAU-13X),[42, 43] iron particles,[44] natural pollen particles,[7] synthetic diamond microparticles,[45] etc.[46] The presence of fillers can efficiently enhance the mechanical properties of the resulting polymers, including the storage modulus, the Young's modulus, and the volume shrinkage, etc.[1, 38] As a class of aluminosilicates, zeolites have lots of micropores and large surface area, which can be used in

various applications, such as drug delivery, adsorption and separation.[42, 47-51] Hence, more and more works about zeolite filled composites or hydrogel composites have been reported in the literature and the resulting composites found potential applications in the field of gas separation, water adsorption, and biomedical engineering.[48, 52, 53] In our previous work,[42] LTA-5A and FAU-13X were used as fillers to be blended with polyethylene glycol diacrylate (PEGDA) to obtain composites with different filler contents through photopolymerization. Compared to the pure PEGDA polymer, the storage modulus (G') of composite was enhanced and the volume shrinkage issue was also improved due to the presence of zeolite. In addition, the composites obtained through direct laser write (DLW) had good water swelling properties, which have also a potential application for 4D printing.

In this work, a chalcone dye was specifically synthesized and employed in photoinitiating system (PIS) for the first time in combination with an amine and an iodonium salt. Then, this PIS was examined for the free radical polymerization (FRP) of polyethylene glycol diacrylate (PEGDA), the cationic photopolymerization (CP) of a benchmark epoxy monomer (EPOX) and their interpenetrating polymer networks (IPNs: PEGDA/EPOX) photopolymerization. In order explore the chemical mechanism, the photochemical reactivity of the chalcone dye was studied, including steady state photolysis, fluorescence quenching, cyclic voltammetry as well as ESR experiments. The photoinitiating ability of the chalcone dye was monitored by Real-time Fourier Transform InfraRed (RT-FTIR) spectroscopy. To evidence the interest of the new formulations, IPN/LTA-5A composites were obtained and their photopolymerization abilities were evaluated by their depth of cure (DOC). Then, these composites were analyzed through scanning electron microscope (SEM), dynamic thermomechanical analysis (DMA), tensile test, water swelling test. 3D printing experiments were also carried out to manufacture 3D patterns. In addition, 3D structured object could have a good 4D behavior under hydrothermal stimuli.

2. Experimental Section

2.1 Materials

The chalcone dye, used as the photoinitiator, was prepared as reported in the supporting information and its structure is presented in the Scheme S1. The cationic photopolymerizable

monomer, 3,4-epoxycyclohexylmethyl-3,4-epoxycyclohexanecarboxylate (Uvacure 1500), was purchased from Allnex and the code in work is EPOX. The free radical photopolymerizable monomer, Polyethylene glycol diacrylate (PEGDA, SR10), was purchased from Sartomer Europe. The zeolite LTA-5A used as the filler in this work was purchased from Sigma-Aldrich, and its characteristic and morphology are listed in Scheme S2.

2.2 Free Radical Photopolymerization (FRP) and Cationic Photopolymerization (CP) Process Monitored by Real Time Fourier Transformed Infrared Spectroscopy (RT-FTIR) under Irradiation of LED with 405 nm

For the photopolymerization experiments, the chalcone (photoinitiator), the amine (EDB, electron donor), and the iodonium salt (Speedcure 938, electron acceptor) were added into the photopolymerizable monomer (0.1wt%/1.5wt%/1.5wt%) in a glass bottle and stirred overnight in the dark, and the mass percent of the three-component photoinitiating system was calculated from the monomer content (Table S1). For the FRP of PEGDA, drops of the homogenous photosensitive formulations were deposited in the laminate between 2 polypropylene films to sandwich the formulation in the middle in order to reduce the O_2 inhibition (thickness ~20 μm), then exposed to irradiation upon LED@405 nm (I_0=100 mW·cm^{-2}) at room temperature. For the CP of EPOX films, the photosensitive resin (thickness ~20 μm) was irradiated under air. The conversion of acrylate of PEGDA and epoxy groups of EPOX were continuously monitored using a RT-FTIR JASCO FTIR 4700 (JASCO, Lisses, France) at the characteristic peaks of 1630 cm^{-1} and 790 cm^{-1} respectively. The conversion of the reactive function was calculated using equation 1 (eq. 1):

$$\textbf{Conversion}\ (\%) = (\mathbf{A_0} - \mathbf{A_t})/\mathbf{A_0} \times \mathbf{100}\% \qquad (1)$$

A_0 is the initial peak area before irradiation and A_t is the peak area after irradiation for a given time t.

2.3 UV-Visible Absorption, Photolysis Property, and Fluorescence Property of Chalcone Dye.

In this work, the UV-visible absorption properties and the photolysis experiments of the proposed dye were investigated through a JASCO V730 UV-visible spectrometer. The chalcone

dye was dissolved in acetonitrile (about 5×10^{-5} M). Furthermore, the concentration Iod and EDB were kept at 0.01 M for the photolysis experiments with a LED with 405 nm. In addition, the fluorescence property of chalcone dye was studied in acetonitrile (about 5×10^{-5} M) with a JASCO FP-6200 spectrofluorometer.

2.4 Cyclic Voltammetry

The redox potentials of the chalcone dye (oxidation potential noted E_{ox} and reduction potential noted E_{red}) was measured as follow. The chalcone dye was dissolved in acetonitrile while using tetrabutylammonium hexafluorophosphate (0.1 M) as the supporting electrolyte (potential vs. Saturated Calomel Electrode, SCE). Free energy change ($\Delta G_{S1}{}^{Iod}$ or $\Delta G_{S1}{}^{EDB}$) for the electron transfer reaction was calculated from equations 2 or 3 (eq. 2 or eq. 3), where E_{ox}, E_{red} and E^*_{S1} are the oxidation potential of the electron donor, the reduction potential of the electron acceptor and the excited state energy level (calculated from the crossing point of UV-visible and fluorescence spectra), respectively.

$$\Delta G^{S1}{}_{Iod} = E_{OX} - (-0.7) - E_{S1} \quad (2)$$

$$\Delta G^{S1}{}_{EDB} = 1.0 - E_{red} - E_{S1} \quad (3)$$

2.5 Electron Spin Resonance-Spin Trapping (ESR-ST) Experiments

A X-band spectrometer (Bruker EMX-plus) was used to carry out the ESR-ST experiments. N_2 saturated Phenyl-*N*-*tert*-butylnitrone (PBN) was selected as the free radical trapping agent, which was irradiated with a LED with 405 nm in room temperature. ESR spectra simulations were performed by WINSIM software.

2.6 Photopolymerization of Zeolite Filled Composites

The three-component photoinitiating system (chalcone dye/Iod/EDB) was mixed with PEGDA and EPOX in glass bottles overnight to obtain the homogeneously resin mixture. Then, the resin mixture and LTA-5A zeolite were added into an opaque vial respectively and mixed with rotation speed at the range of 2000 to 2500 rpm in a High Speedmixer (DAC 150.1 FVZ-K) to obtain homogeneous filled resins, which were stored in the dark before

photopolymerization reactions. All formulations are presented in Table S2 in supporting information.

The cured composites were prepared under the irradiation of the visible UV light (405 nm, 1 W/cm^2) for 60 s. Then, the cured composites were cleaned by acetone to remove the unpolymerized part and the depth of cure (DOC) for the cured composite was measured by an Absolute LCD Digimatic Indicator (Mitutoyo).

2.7 Direct Laser Write (DLW)

The homogeneously filled resins were deposited onto a homemade glass tank (2 mm thickness). Then a computer-controlled and programmed laser diode (Thorlabs with 405 nm, 110 mW·cm^{-2}) with spot size around 50 μm was used for spatial controlled irradiation to produce specific 3D patterns. After the process of DLW, these 3D patterns were cleaned by acetone to remove the uncured monomer. Finally, the printed 3D patterns were observed through a numerical optical microscope (NOM) (DSX-HRSU, OLYMPUS Corp).

2.8 Material Characterization

The zeolite particle size, morphology, and their corresponding composites were investigated using JEOL JSM-7900F scanning electron microscope (SEM). Thermogravimetric analyses (TGA) were carried out using a METTLER-TOLEDO TGA/DSC 3+ thermoanalyzer. 30 mg samples were heated from 30 to 500°C at a scan rate of 10°/min under nitrogen atmosphere (purge of 100 ml/min of N_2 protection gas).

For DMA, all samples were polished to obtain pellets with a thickness of 1 mm, and then experiments were performed on a Viscoanalyser METTLER DMA861 at a frequency of 1.00 HZ. For tensile strain tests, samples were prepared into dumbbell-like samples (1 mm thickness) and were tested by Dynamometer INSTRON 4505 modernized ZWICK.

After DLW, some 3D cross-shaped objects were obtained and then were used for water swelling property characterization. These samples were submerged in distilled water at room temperature (25ºC, 6 h). Then, these samples were taken out periodically and wiped out the water on their surfaces, and were weighted immediately by a precise four-digit balance to

measure the content of water absorbed. The percentage of water swelling property was calculated with the equation 4 (eq.4):

$$R=\frac{m_2-m_1}{m_1}\times 100\% \quad (4)$$

Where m_2 is the weight of the sample after water swelling, and m_1 is the weight of the dried sample.

3. Results and Discussion

3.1 Synthesis of the Chalcone Dye

The chalcone dye was synthesized in one step, by a Claisen Schmidt condensation in basic conditions, involving 2,4,5-trimethoxybenzaldehyde and 3',4',5'-trimethoxyacetophenone. The chalcone directly precipitated in the solvent reaction, namely ethanol so that the product could be recovered in pure form by a simple filtration. The chalcone was isolated as a yellow powder in 88% yield (See Scheme XX)

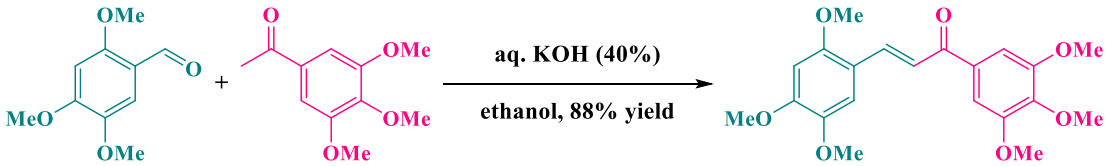

Scheme XX. Synthetic route to the chalcone dye.

3.2 Light Absorption Property of Chalcone Dye

The UV-visible absorption spectrum of the chalcone dye in acetonitrile is shown in Figure S1, and its absorption maximum value (λ_{max}) and molar extinction coefficient (ε_{max}) at λ_{max} and its extinction coefficient at 405 nm (ε_{405nm}) are summarized in Table S3. The maximum absorption peak appeared at 312 nm and 387 nm, which guaranteed a good overlap with the emission spectra of the LED with 405 nm used in this work. Remarkably, this chalcone dye had a high extinction coefficient (13570 $M^{-1}cm^{-1}$ at 405 nm).

3.3 Free Radical Photopolymerization (FRP) and Cationic Photopolymerization (CP)

As shown in Figure 1.a and Table S4, for the polymerizations of PEGDA and EPOX monomer, the photoinitiation ability of three-compound PIS (chalcone dye/Iod/EDB) was studied by RT-FTIR in thin films and thick films under irradiation with LED@405 nm and at room temperature. For PEGDA, the final acrylate function conversions of thin film and thick film were 91% and 97% respectively. For EPOX, the final epoxy function conversions of thin film and thick film were 15% and 62% respectively. For both PEGDA and EPOX, their final conversions of thick films were both higher than that of their corresponding thin films. As shown in Table S4, the polymerization profile of this PIS was much better than the blank control, which was only initiated by the co-initiator (1.5 wt% Iod and 1.5 wt% EDB). Obviously, with the photoinitiation of the blank control, the final conversion for EPOX polymer was 0 %. Hence, it demonstrates the huge effect of the presence of the chalcone dye for the photopolymerization process.

Photopolymerization of interpenetrating polymer networks (IPN) consisting in 50 wt% PEGDA and 50 wt% EPOX was also studied by RT-FTIR in thin films and thick films under irradiation with LED@405 nm and at room temperature. The results are presented in Figure 1 and Table S4. With the photoinitiation of PIS, the final conversion of PEGDA in thin film and thick film were 76 % and 96 % respectively, and that of EPOX in thin film and thick were respectively of 43 % and 36 %. It is clear that PEGDA has a stable final monomer conversion in the thick films both of pure PEGDA (97 %) and PEGDA in IPN (96 %). The final conversions of pure PEGDA in thin film and pure EPOX in thick film both decreased, compared to their corresponding IPNs. Furthermore, compared to the blank control, presence of the chalcone dye can improve the photopolymerization of the monomers in IPN (the higher final conversion). Therefore, it is interesting to investigate further on this PIS (chalcone dye/Iod/EDB) upon photopolymerization, especially on the photopolymerization of IPN.

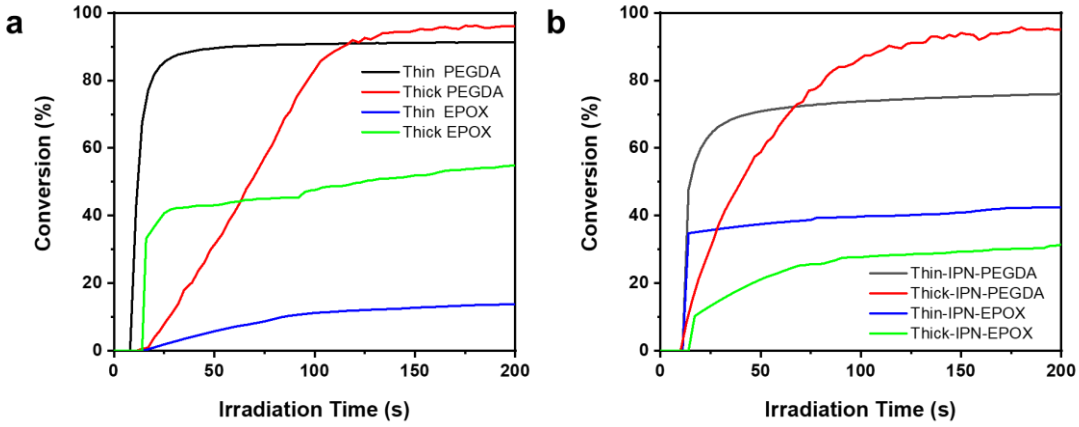

Figure 1. Photopolymerization profiles for acrylate or epoxy functions in PEGDA, EPOX or IPNs (conversion of C=C bonds or epoxy functions (%) vs irradiation time (s)) initiated by the chalcone dye, Iod and EDB in laminate both in thin films and thick films (Chalcone dye : Iod : EDB=0.1 wt% : 1.5 wt% : 1.5 wt%. (a) Pure polymer of PEGDA or EPOX; (b) IPN consisting of PEGDA/EPOX (50%/50%). The irradiation started for t = 10 s.

3.4 Photochemical Reactivity

Steady-state photolysis experiments were carried out to study the interaction activity of the chalcone dye with the two additives, namely Iod or EDB in acetonitrile. There were obvious and significant declines of the UV-visible absorption intensity for the chalcone dye in the corresponding three-component system (chalcone dye/Iod/EDB) and two-component system (chalcone dye/Iod and chalcone dye/EDB). All of them completely decomposed within 25 s (See Figure 2.a - 2.d). As shown in Figure 2.e, the two-component system (chalcone dye/Iod) had the highest consumption (72.4 %) when the irradiation time was 20 s, even higher than that observed for the three-component system (chalcone dye/Iod/EDB) (48.5 %). Conversely, the two-component system (chalcone dye/EDB) and the chalcone alone both had the lowest consumptions (37.3 %, 38.8 % respectively). Therefore, the interaction of the chalcone dye in the two-component chalcone dye/Iod system was more efficient than that observed in the chalcone dye/EDB combination. Therefore, the photoinitiation process for the three-component system can consist of two reaction parts: (1) the combination of the chalcone dye and the iodonium salt (Iod), and (2) the combination of the chalcone dye and the aromatic amine (EDB). The proposed mechanism will be shown below in Scheme 1.

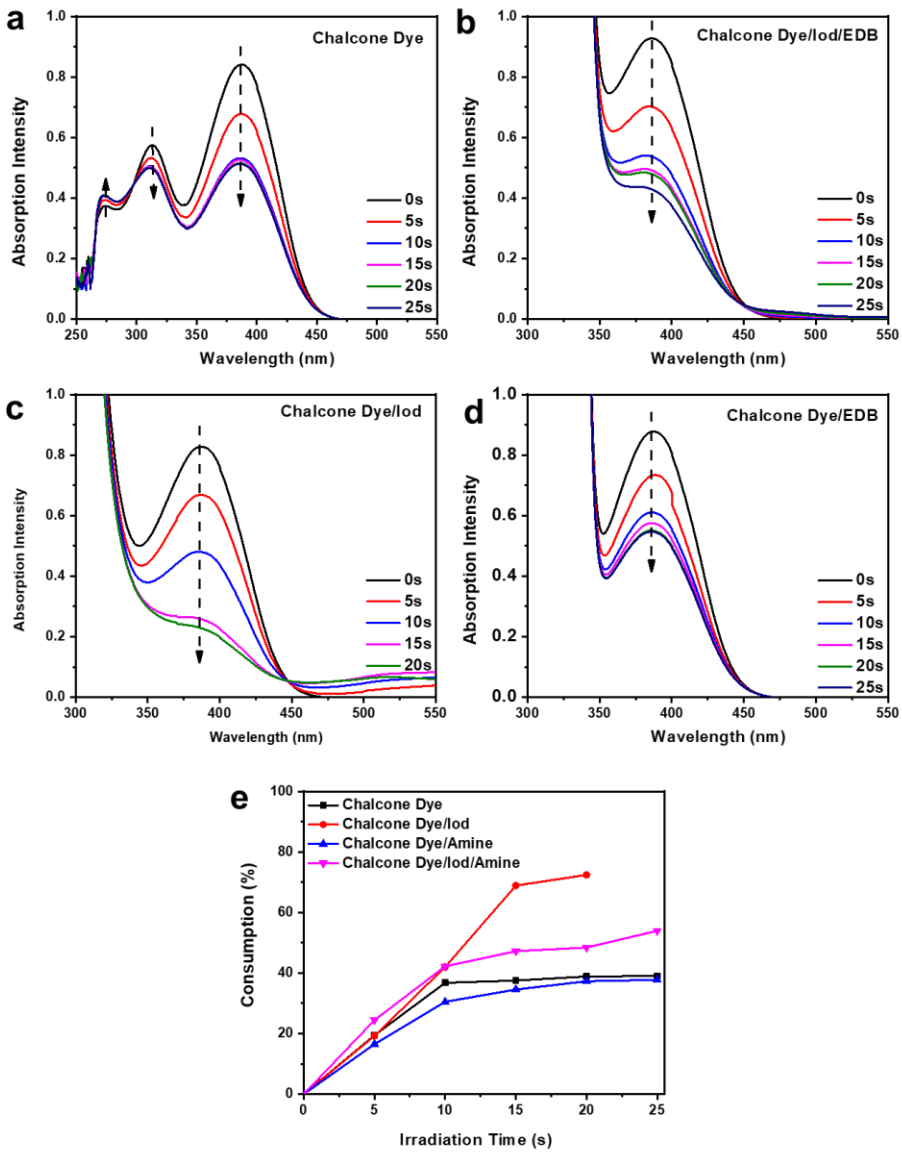

Figure 2. Photolysis of (a) chalcone dye (5×10^{-5} M) in acetonitrile, (b) chalcone dye (5×10^{-5} M)/Iod (0.01 M)/EDB (0.01 M), (c) chalcone dye (5×10^{-5} M)/Iod (0.01 M), (d) chalcone dye (5×10^{-5} M)/EDB (0.01 M), (e) consumption of the chalcone dye during the photolysis process.

Fluorescence quenching experiments for the chalcone dye were conducted in acetonitrile to see the theoretical feasibility of the interaction of chalcone dye/Iod and chalcone dye/EDB. As shown in Figure 3.a and Figure 3.c, intensity of the emission peak of the chalcone dye decreased with the continuous addition of Iod or EDB. Therefore, Iod and EDB could both act as quenchers for the chalcone excited singlet state. However, based on the changes of intensity of emission, the combination of chalcone dye/Iod was better than that of the chalcone dye/EDB combination. Furthermore, linear curves could be fitted from the fluorescence quenching

processes (Figure 3.b and Figure 3.d), and their corresponding values of the Stern-Volmer coefficients (K_{sv}, the slope of the curve) are also presented in Table 1 (chalcone dye/Iod interaction $K_{sv}^{Iod} = 63\ M^{-1}$, chalcone dye/EDB $K_{sv}^{EDB} = 6\ M^{-1}$). Based on equation 5 and equation 6 (eq. 5 and eq. 6), the electron transfer quantum yield in the excited singlet state (Φ_{et}) for the expected electron transfer reaction between the chalcone and Iod (0.66) or EDB (0.34) was calculated in Table 1. It is also obvious to see that the electron transfer quantum yields of chalcone dye/Iod (Φ_{et}^{Iod}) had a higher reactivity than that of chalcone dye/EDB (Φ_{et}^{EDB}). Hence, the combination of chalcone dye/Iod had a higher reactivity than that of chalcone dye/EDB.

$$\mathbf{\Phi_{et}^{Iod} = K_{sv}^{Iod} * [Iod]/(1 + K_{sv}^{Iod} * [Iod])} \quad \mathbf{(5)}$$

$$\mathbf{\Phi_{et}^{Iod} = K_{sv}^{EDB} * [EDB]/(1 + K_{sv}^{EDB} * [EDB])} \quad \mathbf{(6)}$$

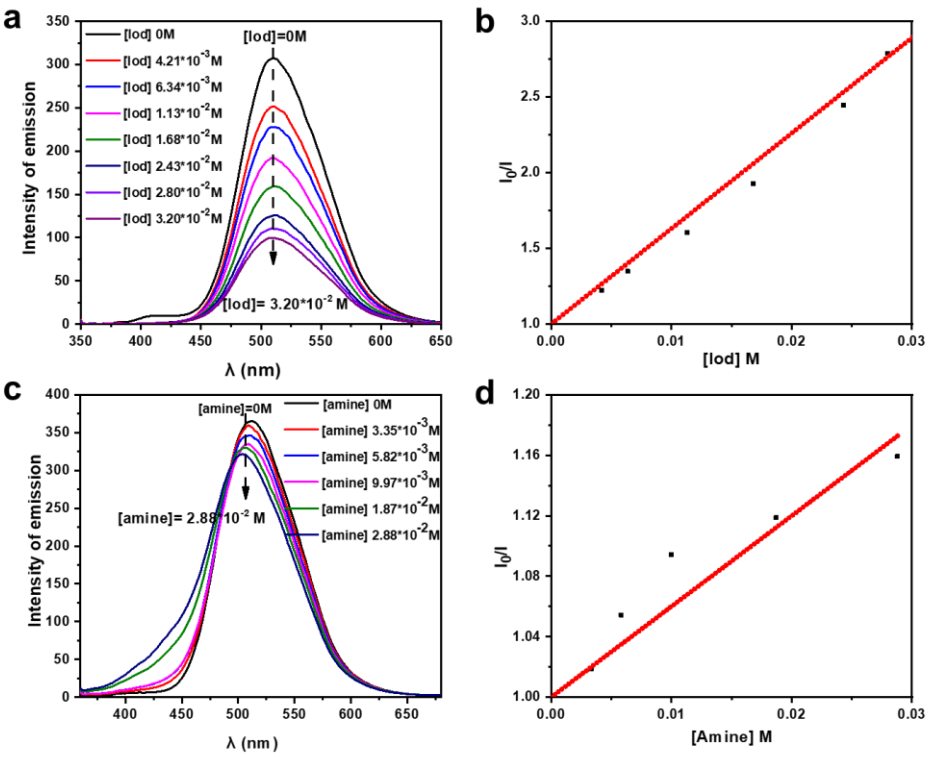

Figure 3. (a) Fluorescence quenching of chalcone dye by Iod in acetonitrile; (b) Stern-Volmer treatment for chalcone dye/Iod fluorescence quenching; (c) Fluorescence quenching of chalcone dye by EDB in acetonitrile; (d) Stern-Volmer treatment for chalcone dye/EDB fluorescence quenching.

Table 1. Parameters characterizing the electron transfer reactions for the chalcone dye in acetonitrile.

K_{sv}^{Iod} (M^{-1})	K_{sv}^{EDB} (M^{-1})	Φ_{et}^{Iod}	Φ_{et}^{EDB}	E_{S1} (eV)	E_{ox} (eV)	E_{red} (eV)	ΔG_{S1}^{Iod}	ΔG_{S1}^{EDB}
63	6	0.66	0.34	2.76	1.12	-1.59	-0.94	-0.17

As shown in Figure S2.a, the first singlet excited state energy (E_{S1}) of the chalcone dye was evaluated from the crossing point of the UV-absorption curve and the fluorescence spectra curve in acetonitrile (E_{S1} = 2.76 eV, shown in Table 1). The redox potentials of the chalcone dye (E_{ox} and E_{red}) were obtained in acetonitrile by cyclic voltammetry to study the mechanism of the chalcone dye based photoinitiating system (See Figure S2.b). The half peak oxidation potential (E_{ox} = 1.12 eV), and the reduction potential (E_{red} = - 1.59 eV) for the chalcone dye are gathered in Table 1. The free energy changes ΔG_{S1}^{Iod} and ΔG_{S1}^{EDB} for electron transfer reaction of chalcone dye/Iod (ΔG_{S1}^{Iod} = - 0.94) and chalcone dye/EDB (ΔG_{S1}^{EDB} = - 0.17) were both calculated by equation (eq. 2 and eq. 3) and presented in Table 1. Due to $\Delta G < 0$, it indicated the theoretical feasibility of these electron transfer reactions.

The different generated radicals were detected by the ESR-spin trapping experiments done on the chalcone dye/Iod and chalcone dye/EDB solutions under N_2 in *N*-phenyl-*tert*-butyl nitrone (PBN) as the spin trap agent. As shown in Figure 4.a and 4.b, for the chalcone dye/Iod combination, the PBN/aryl radical adducts were clearly observed (a_N = 14.4 G and a_H = 2.2 G, in agreement with literature data). As presented in Figure 4.c and 4.d, for the chalcone dye/EDB combination, the hyperfine coupling constants of PBN radical adducts were a_N = 14.4 G and a_H = 2.2 G. In addition, some very minor signals ascribed to PBNox (the oxidized form of PBN) were observed and it can be due to side reactions. Thus, the feasibility of the chemical mechanisms mentioned above has clearly been proved, i.e., the photoinitiation process for the three-component system can consist of two reaction parts: (1) the combination of the chalcone dye and the iodonium salt (Iod), and (2) the combination of the chalcone dye and the aromatic amine (EDB). r_1 – r_5 in Scheme 1 demonstrate the formation of the initiating species for the free radical photopolymerization (FRP) and the cationic photopolymerization (CP).

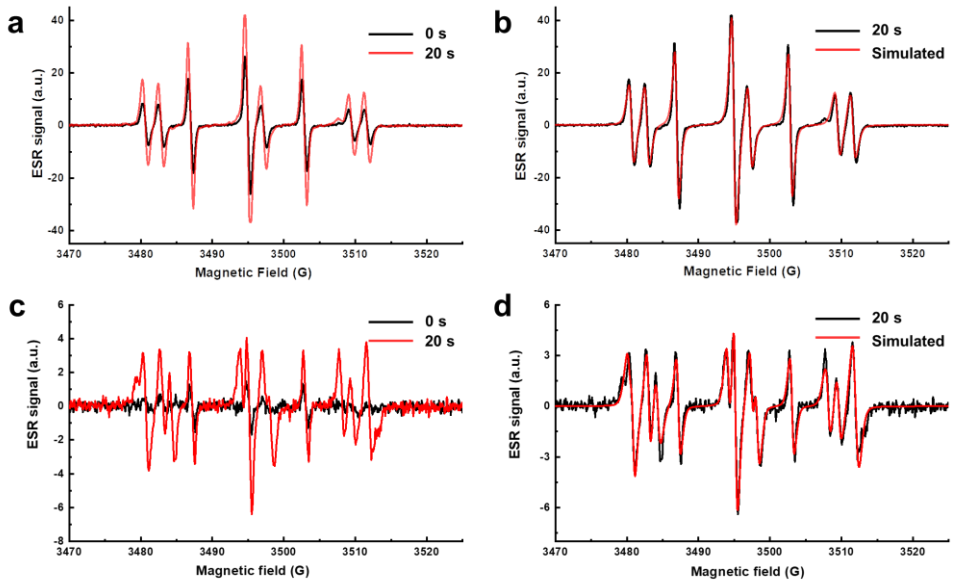

Figure 4. ESR spectra obtained from ESR-spin trapping experiment using PBN = 2 mg/mL (as spin trap agent); Iod (Speedcure 938) = 12.6 mg/mL; EDB (Speedcure EDB) = 12.6 mg/mL and the chalcone dye = 0.8 mg/mL in acetonitrile under N_2. (a) chalcone dye/Iod Irradiation time = 0 s (black) and = 20 s (red) spectra; (b) chalcone dye /Iod Irradiation time = 20 s (black) and simulated (red) spectra; (c) chalcone dye /EDB Irradiation time = 0 s (black) and = 60 s (red) spectra; (d) chalcone dye/EDB Irradiation time = 60 s (black) and simulated (red) spectra.

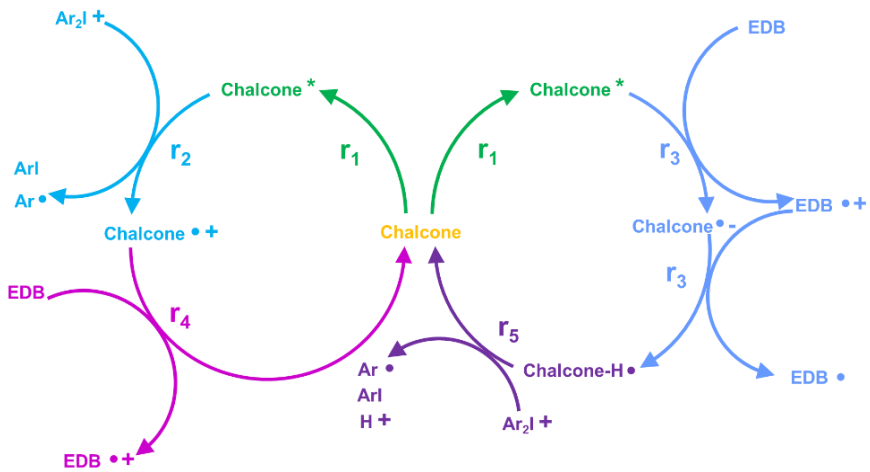

Scheme 1. Proposed photoinitiation mechanisms.

3.5 Photopolymerization of Zeolite Filled IPN Composites

The depth of cure (DOC) is a very important property of light-cured composites, which is defined here as the thickness of composite cured adequately under LED@405 nm. In Figure 5.b, the mechanism of photopolymerization of IPN/LTA-5A composites has been presented, and the crosslink of zeolite and IPN could be obtained after photopolymerization (LTA@405nm,

in air and at room temperature).

As shown in Figure 5.a, the DOC values showed major differences depending of the type of photopolymerizations and the filler (LTA-5A) contents. Normally, the transmittance of the filled samples decreases with the increase of the filler content, and the DOC values gradually decrease (See DOC values of PEGDA based composite in Figure 5.a). However, it is interesting to note that the LTA-5A filled IPN composites have the opposite results for DOC: the presence of LTA-5A improved the photopolymerization in depth. As shown in Figure 5.a, With the increasing filler content, the corresponding DOC values also increased correspondingly (from 1.4 mm for pure IPN to 2.7 mm for IPN-50%, increased by ca. 90 %). After photopolymerization, the presence of LTA-5A zeolite could help the IPN to have a better crosslink and improve the 3D structure of the polymer network. Based on DOC values, it is interesting to note that the DOC of IPN/LTA-5A composites with higher filler content (30 wt% and 50 wt%) was better than that of PEGDA/LTA-5A composites. Particularly, the DOC of IPN-50%LTA (2.7 mm) was more than 50 % higher than that of PEGDA-50%LTA (1.7 mm). Therefore, the presence of LTA-5A can significantly improve the photopolymerization ability of IPN. It has to be noticed that such an improvement is reported for the first time for the DOC of composites, with an increase of the DOC with the filler content.

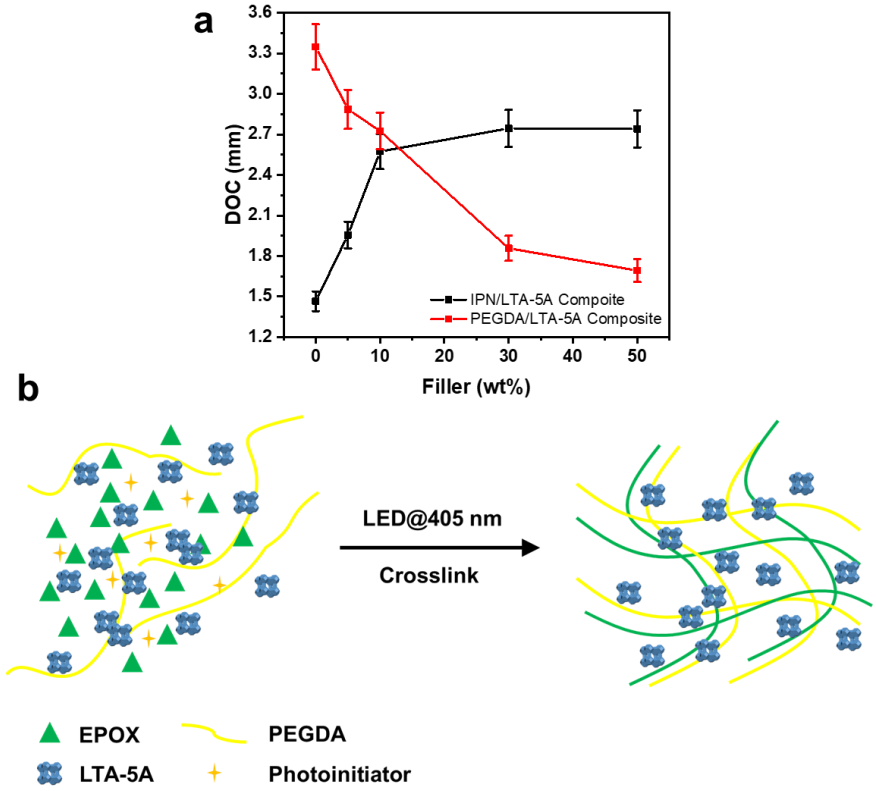

Figure 5. (a) DOC for IPN/LTA-5A composites and PEGDA/LTA-5A composites; (b) the mechanism of the photopolymerization for IPN/LTA-5A composites.

The LTA-5A zeolite powder and IPN/LTA-5A composites were observed by scanning electron microscope (SEM). As shown in Scheme S2, LTA-5A crystals (the average size (diameter) of 2.6-2.7 μm) have easily recognizable well-shaped cubic morphology. SEM images of different IPN/LTA-5A composites are presented in Figure S3. The surface of the pure IPN was not flat with some protruding parts, and the image for its cross-section shows that there were many homogeneous bubble-like parts, which might be due to the crosslink of IPN (See Figure S3.b). This similar distribution also could be observed in Figure S3.d (IPN-5%LTA) and Figure 6.f (IPN-10%LTA). It is much easier to observe more LTA-5A on the surface and the cross-section of IPN/LTA-5A composites, when more LTA-5A was added (See Figure S3.g - S3.j). Intimate contact between the LTA-5A and IPN in general with a rather good dispersion on the faces, as well as along the cross-section. Hence, homogeneous composites could be obtained through photopolymerization process.

3.6 Mechanical Properties of Zeolite Filled IPN Composites

Lack of good mechanical properties and functions was the normal flaw of pure polymer after photopolymerization or 3D printing. The introduction of filler can significantly improve the mechanical properties of the resulting composite. Hence, dynamical thermomechanical analyses (DMA) and tensile tests were carried out for IPN/LTA-5A composites.

As shown in Figure 6.b, compared to the pure IPN, the storage modulus (G') of IPN/LTA-5A composites at 25 ^{o}C increased obviously (from 1.3 MPa to 7.1 MPa, increased by ca. 445 %) with the increase of the content of LTA-5A (from 0 wt% to 50 wt%). In fact, the well-dispersed LTA-5A zeolite with good interactions with the IPN clearly improved the storage modulus (G'), due to the increase of constrains of segmental motions of the polymeric chain in IPN. Furthermore, the small size of LTA-5A did not create large stress concentrations, and they even could improve the ductility.

As shown in Figure 6.a, different IPN/LTA-5A composites with the same dumbbell shape were manufactured for tensile test study. With the increase of the filler content, the transparency of composites gradually decreased. The tensile test results were presented in Figure 6.c - 6.e. Compared to tensile strain and tensile strength of the pure IPN (6.1 % and 0.3 MPa, respectively), that of the IPN/LTA-5A composite both increased with the increase of the filler content, especially the tensile strength of IPN-50%LTA (1.3 MPa) increased by ca. 430 %. Simultaneously, the Young's modulus also increased with the increase of the filler content. Compared to the lowest Young's modulus value of the pure IPN (5.1 MPa), IPN-50%LTA had the highest value (34.7 MPa), which increased by ca. 580 %. According to the results of tensile strength and Young's modulus, when the filler content reached 50 wt%, it did not have a significant hindrance on the photopolymerization of IPN. Therefore, the introduce of LTA-5A zeolite could drastically improve the mechanical properties of IPN.

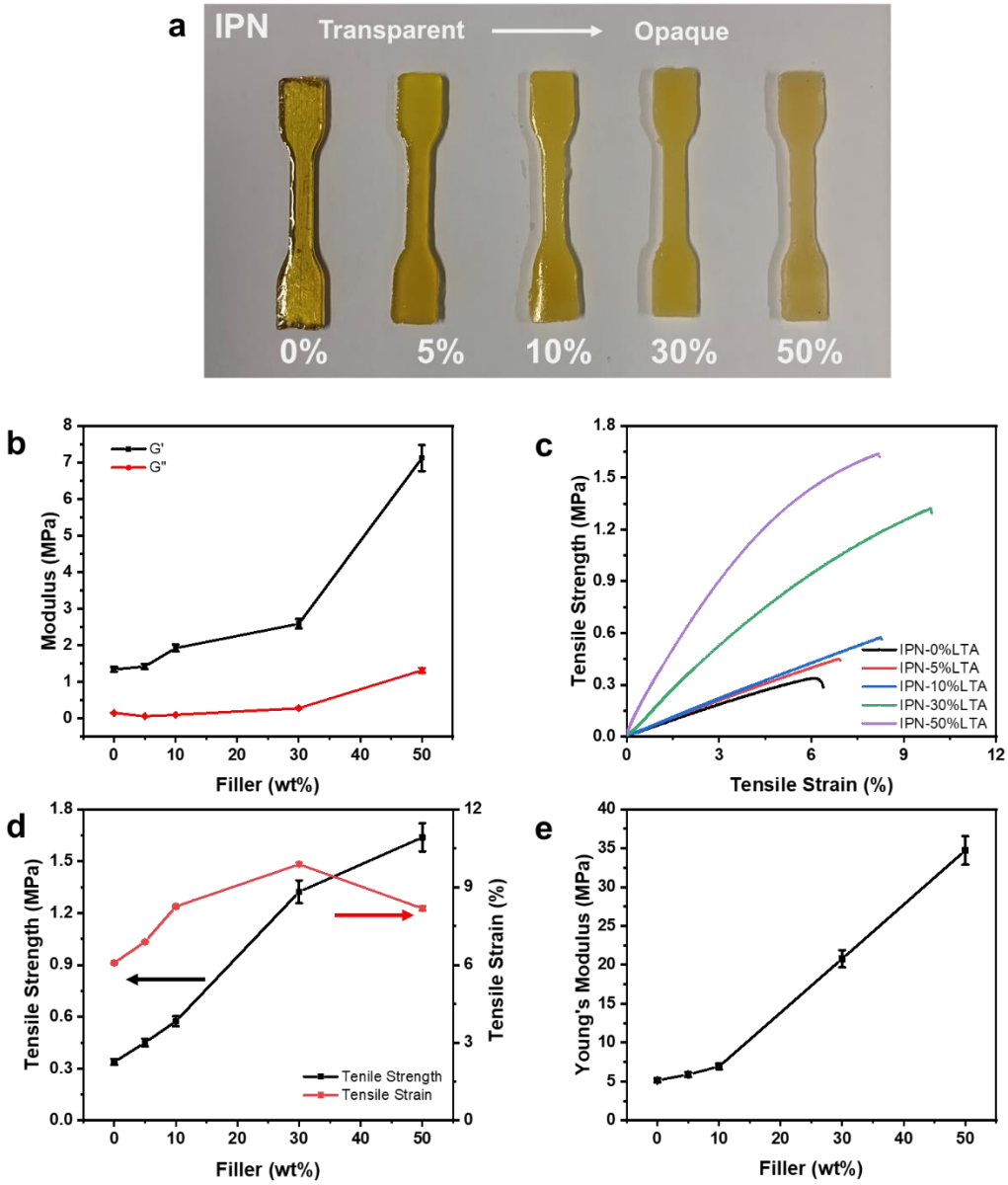

Figure 6. (a) Dumbbell-shaped objects of IPN/LTA-5A composites for tensile test; (b) dynamic thermomechanical analysis for IPN/LTA-5A composites; (c) tensile test results (Tensile strength vs Tensile strain); (d) tensile test results (tensile strength and tensile strain vs filler content); (e) The Young's modulus of IPN/LTA-5A composites vs. filler content.

3.7 Direct Laser Write (DLW)

Based on the results presented above, the three-component photoinitiating system (chalcone dye/Iod/EDB) had a good photoinitiation ability to produce pure IPN and IPN/LTA-5A composites by photopolymerization. Hence, direct laser write (DLW), a technique of 3D printing, was used to generate different 3D patterns (See Figure 7.a, 7.c and 7.e). Particularly, when the filler content was 50 wt%, 3D patterns also could be obtained successfully through

DLW. As the color patterns morphology presented in Figure 7.b, 7.d and 7.f, it can be clearly observed that these 3D patterns have good resolution and flat surfaces.

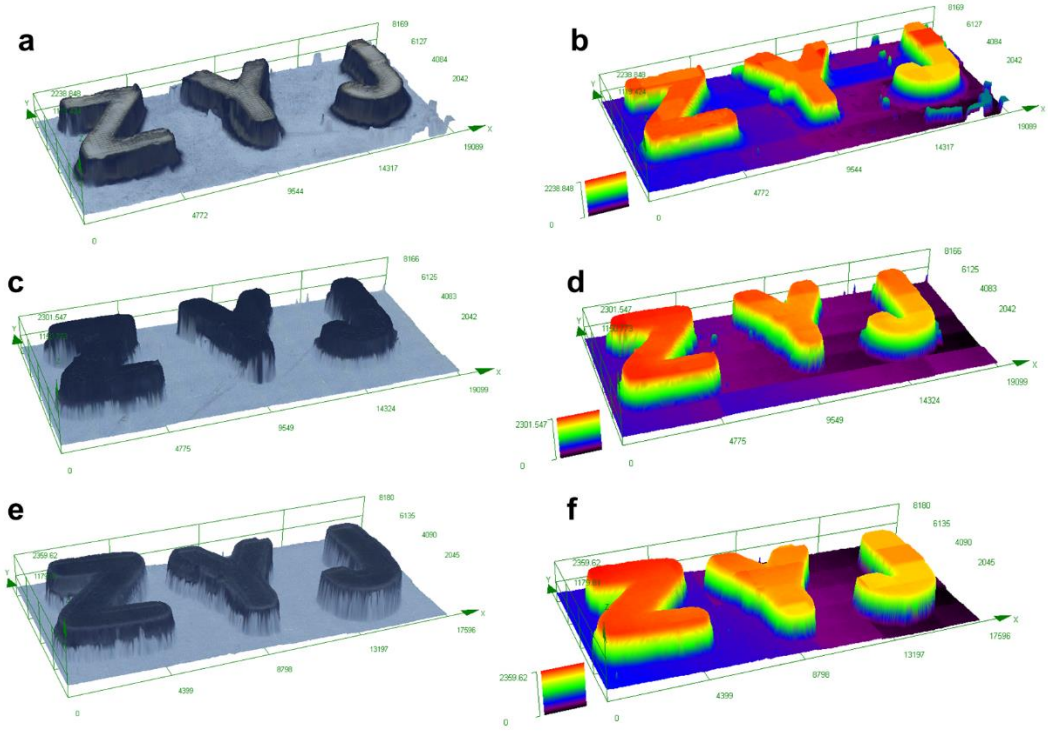

Figure 7. The numerical optical microscopy images for IPN-0%LTA, IPN-30%LTA and IPN-50%LTA after direct laser writing (DLW). (a), (c) and (e): top surface morphology; (b), (d) and (f): color patterns.

3.8 Functions of IPN/LTA-5A Composites

As we know, PEG based polymers normally have a good water swelling property. Since the investigated IPNs consist of a mixture of PEGDA and EPOX, water swelling tests were carried out to quantitatively illustrate the properties of IPN/LTA-5A composites with different filler contents. As shown in Figure 8.a, the water swelling ratio decreased with the increasing filler content. When the filler content of LTA-5A increased from 0 wt% to 50 wt%, the swelling ratio decreased from 76.0 wt% to 40.5 wt%. This could be due to the presence of LTA-5A zeolite, which decreased the content of polymer.

The images of the 3D patterns composites (pattern “Z”) with different filler contents at different processes of water swelling was presented in Figure 8.b, including before water swelling, after water swelling@ room temperature for 6 h, and after evaporation@40 ºC for 1 h. However, due to the higher swelling ratio, some cracks or irrecoverable deformation

(highlighted in red circles) appeared during the evaporation process on the surface of 3D patterns with low filler content (0 wt%, 5 wt% and 10 wt%). Interestingly, it is easy to observe that 3D patterns (letter "Z") (IPN-30%LTA and IPN-50%LTA) expanded after water swelling and returned close to their origin shapes after evaporation, and the processes of water swelling and water evaporation could be accomplished many times. This means that the 3D patterns with high filler contents obtained through DLW can achieve repeated regular deformation under the influence of the presence of water. Hence, this stable property of IPN-30%LTA and IPN-50%LTA provided the potential possibility for the 4D printing behavior under the hydrothermal stimuli.

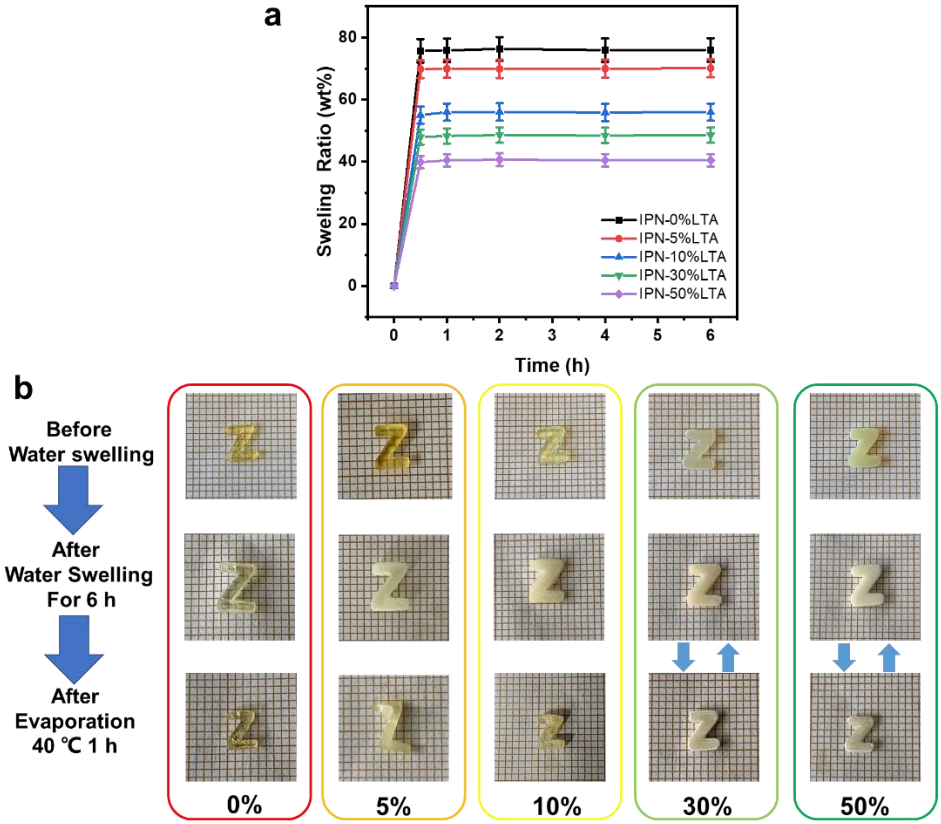

Figure 8. Water swelling for IPN/LTA composites with different filler contents: 0 wt%, 5 wt%, 10 wt%, 30 wt% and 50 wt%. (a) water swelling ratio vs swelling time; (b) The swelling process consisting in 3 steps: before water swelling, after water swelling (6 h), after evaporation (40 ºC for 1 h). Each small square in the background of each photo is the standard 1mm x 1mm size.

Normally, 4D printing is regarded as giving to a printed structure the ability to change its

form, color or function with time (t) under stimulus of temperature, water, light, electricity, etc. Based on the 3D printing technique, 4D printing technique has a rapid development in recent years. Hence, as shown in Figure 9.a, a 3D cross-shaped object and a 3D strip-shaped object were designed and manufactured, and then the 4D printing behavior was obtained under hydrothermal stimuli.

As shown in Figure 9.b and 9.c, the 3D strip-shaped object (IPN-50%LTA) and the 3D cross-shaped object (IPN-50%LTA) after water swelling were put in oven at 90 ºC for evaporation. As shown in Video S1 and Video S2, during the evaporation process within 10 min, the central part of these two objects was raised or the corners of the object curled up. Then, these two objects returned to the unfolded state quickly when they were put in water and after water evaporation. Simultaneously, this obvious shape memory change could be repeated for several times without any cracks on the surfaces of these objects or irrecoverable deformation (See Video S3). Therefore, the significant 4D printing behavior can be exhibited under the hydrothermal stimuli.

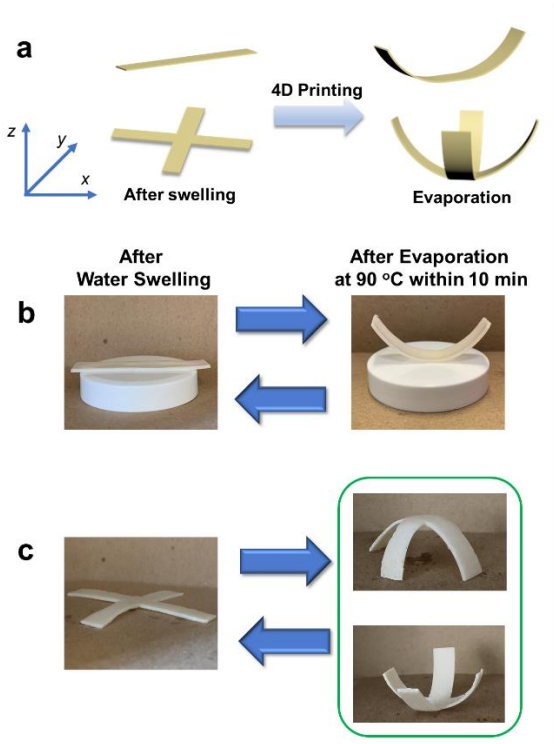

Figure 9. Water swelling for IPN/LTA composites with different filler contents: 0 wt%, 5 wt%, 10 wt%, 39 wt% and 50 wt%. (a) water swelling ratio vs swelling time; (b) The swelling process consisting in 3 steps: before water swelling, after water swelling (6 h), after evaporation (40 ºC

for 1 h). Each small square in the background of each photo is the standard 1mm x 1mm size.

4. Conclusion

In this work, a chalcone dye was synthesized, and its photoinitiation ability was also examined. To clarify the relevant photochemical mechanism steady state photolysis and fluorescence experiments were carried out on PIS (chalcone dye/Iod/EDB) with LED@405 nm. Furthermore, the chemical mechanism was confirmed by ESR experiments. This PIS could effectively initiate both free radical photopolymerization (FRP) and cationic photopolymerization (CP) in interpenetrating polymer network (IPN, PEGDA/EPOX). The depth of cure values for these homogeneous IPN/LTA-5A composites could kept increasing with the increased filler contents. The introduction of LTA-5A was very effective in improving the mechanical properties for IPN. Simultaneously, 3D patterns with good resolution and flat surface were manufactured through direct laser write (DLW), and the presence of large amount of LTA-5A in 3D patterns make sure the composite without break during the water swelling process. In addition, a good and stable 4D printing behavior under hydrothermal stimuli can be repeated on IPN/LTA-5A composites. This work not only expand our understanding about the chemical mechanisms of chalcone dye based PIS on interpenetrating polymer network (IPN) and its corresponding filled composites, but also find important potential applications of photopolymerization reactions in the field of 3D printing, 4D printing, microlithography, and the design of biocompatible materials for drug release, etc.

Corresponding Authors

Jacques Lalevée, jacques.lalevee@uha.fr

Angélique Simon-Masseron, angelique.simon-masseron@uha.fr

Frédéric Dumur, frederic.dumur@univ-amu.fr

Notes

The authors declare no competing financial interest.

Acknowledgments

Authors wish to thank the Region Grand Est (France) for the grant “MIPPI-4D”.

Data availability statement

The raw/processed data required to reproduce these findings can be furnished on demand.

Reference

1. Zhang, Y.; Xu, Y.; Simon-Masseron, A.; Lalevee, J., Radical photoinitiation with LEDs and applications in the 3D printing of composites. *Chemical Society Reviews* **2021,** *50* (6), 3824-3841.

2. Lee, S. J.; Zhu, W.; Nowicki, M.; Lee, G.; Heo, D. N.; Kim, J.; Zuo, Y. Y.; Zhang, L. G., 3D printing nano conductive multi-walled carbon nanotube scaffolds for nerve regeneration. *Journal of Neural Engineering* **2018,** *15* (1), 016018.

3. Yu, F.; Han, X.; Zhang, K.; Dai, B.; Shen, S.; Gao, X.; Teng, H.; Wang, X.; Li, L.; Ju, H.; Wang, W.; Zhang, J.; Jiang, Q., Evaluation of a polyvinyl alcohol-alginate based hydrogel for precise 3D bioprinting. *Journal of Biomedical Materials Research Part A* **2018,** *106* (11), 2944-2954.

4. Halevi, O.; Chen, T.-Y.; Lee, P. S.; Magdassi, S.; Hriljac, J. A., Nuclear wastewater decontamination by 3D-printed hierarchical zeolite monoliths. *RSC Advances* **2020,** *10* (10), 5766-5776.

5. Zhang, H.; Wang, P.; Zhang, H.; Yang, H.; Wang, H.; Zhang, L., Structured zeolite monoliths with ultrathin framework for fast CO2 adsorption enabled by 3D printing. *Industrial & Engineering Chemistry Research* **2020,** *59* (17), 8223-8229.

6. Lim, C. W. J.; Le, K. Q.; Lu, Q.; Wong, C. H., An overview of 3-D printing in manufacturing, aerospace, and automotive industries. *IEEE Potentials* **2016,** *35* (4), 18-22.

7. Zhang, Y.; Chen, H.; Liu, S.; Josien, L.; Schrodj, G.; Simon-Masseron, A.; Lalevée, J., Photopolymerization of pollen based biosourced composites and applications in 3D and 4D printing. *Macromolecular Materials and Engineering* **2021**.

8. Choong, Y. Y. C.; Maleksaeedi, S.; Eng, H.; Wei, J.; Su, P.-C., 4D printing of high performance shape memory polymer using stereolithography. *Materials & Design* **2017,** *126*, 219-225.

9. Salimon, A. I.; Senatov, F. S.; Kalyaev, V.; Korsunsky, A. M., Shape memory polymer blends and composites for 3D and 4D printing applications. In *3D and 4D Printing of Polymer Nanocomposite Materials*, 2020; pp 161-189.

10. Zhang, Z.; Corrigan, N.; Bagheri, A.; Jin, J.; Boyer, C., A versatile 3D and 4D printing system through photocontrolled raft polymerization. *Angewandte Chemie International Edition* **2019,** *58* (50), 17954 –17963.

11. Choi, J.; Kwon, O. C.; Jo, W.; Lee, H. J.; Moon, M.-W., 4D printing technology: A review. *3D Printing and Additive Manufacturing* **2015,** *2* (4), 159-167.

12. Gladman, A. S.; Matsumoto, E. A.; Nuzzo, R. G.; Mahadevan, L.; Lewis, J. A., Biomimetic 4D Printing. *Nature Materials* **2016,** *15* (4), 413-8.

13. Piedrahita-Bello, M.; Angulo-Cervera, J. E.; Courson, R.; Molnár, G.; Malaquin, L.; Thibault, C.; Tondu, B.; Salmon, L.; Bousseksou, A., 4D printing with spin-crossover polymer composites. *Journal of Materials Chemistry C* **2020,** *8* (18), 6001-6005.

14. Ahmed, A. A.; Musbah, A.; Atiyah, A., 4D printing technology: A revolution across manufacturing. *International Journal of Mechanical and Industrial Technology* **2020,** *7* (2), 45-51.

15. Lalevée, J.; Fouassier, J.-P., *Photopolymerisation Initiating Systems*. Royal Society of Chemistry: 2018.

16. Baralle, A.; Garra, P.; Graff, B.; Morlet-Savary, F.; Dietlin, C.; Fouassier, J. P.; Lakhdar, S.; Lalevée, J., Iodinated polystyrene for polymeric charge transfer complexes: toward high-performance near-UV and visible light macrophotoinitiators. *Macromolecules* **2019,** *52* (9), 3448-3453.

17. Garra, P.; Fouassier, J. P.; Lakhdar, S.; Yagci, Y.; Lalevée, J., Visible light photoinitiating systems by charge transfer complexes: photochemistry without dyes. *Progress in Polymer Science* **2020,** *107*.

18. Dietlin, C.; Schweizer, S.; Xiao, P.; Zhang, J.; Morlet-Savary, F.; Graff, B.; Fouassier, J.-P.; Lalevée, J., Photopolymerization upon LEDs: New photoinitiating systems and strategies. *Polymer Chemistry* **2015,** *6* (21), 3895-3912.

19. Mokbel, H.; Graff, B.; Dumur, F.; Lalevee, J., NIR sensitizer operating under long wavelength (1064 nm) for free radical photopolymerization processes. *Macromolecular Rapid Communications* **2020,** *41* (15), 2000289-2000293.

20. Garra, P.; Dietlin, C.; Morlet-Savary, F.; Dumur, F.; Gigmes, D.; Fouassier, J.-P.; Lalevée, J., Photopolymerization processes of thick films and in shadow areas: A review for the access to composites. *Polymer Chemistry* **2017,** *8* (46), 7088-7101.

21. Tasdelen, M. A.; Lalevée, J.; Yagci, Y., Photoinduced free radical promoted cationic polymerization 40 years after its discovery. *Polymer Chemistry* **2020,** *11* (6), 1111-1121.

22. Launay, V.; Caron, A.; Noirbent, G.; Gigmes, D.; Dumur, F.; Lalevée, J., NIR organic dyes

as innovative tools for reprocessing/recycling of plastics: Benefits of the photothermal activation in the near-infrared range. *Advanced Functional Materials* **2020,** *31* (7).

23. Liu, S.; Brunel, D.; Noirbent, G.; Mau, A.; Chen, H.; Morlet-Savary, F.; Graff, B.; Gigmes, D.; Xiao, P.; Dumur, F.; Lalevée, J., New multifunctional benzophenone-based photoinitiators with high migration stability and their applications in 3D printing. *Materials Chemistry Frontiers* **2021,** *5* (4), 1982-1994.

24. Dietlin, C.; Trinh, T. T.; Schweizer, S.; Graff, B.; Morlet-Savary, F.; Noirot, P.-A.; Lalevée, J., Rational design of acyldiphenylphosphine oxides as photoinitiators of radical polymerization. *Macromolecules* **2019,** *52* (20), 7886-7893.

25. Han, W.; Fu, H.; Xue, T.; Liu, T.; Wang, Y.; Wang, T., Facilely prepared blue-green light sensitive curcuminoids with excellent bleaching properties as high performance photosensitizers in cationic and free radical photopolymerization. *Polymer Chemistry* **2018,** *9* (14), 1787-1798.

26. Xiao, P.; Zhang, J.; Dumur, F.; Tehfe, M. A.; Morlet-Savary, F.; Graff, B.; Gigmes, D.; Fouassier, J. P.; Lalevée, J., Visible light sensitive photoinitiating systems: Recent progress in cationic and radical photopolymerization reactions under soft conditions. *Progress in Polymer Science* **2015,** *41*, 32-66.

27. Liu, S.; Zhang, Y.; Sun, K.; Graff, B.; Xiao, P.; Dumur, F.; Lalevée, J., Design of photoinitiating systems based on the chalcone-anthracene scaffold for LED cationic photopolymerization and application in 3D printing. *European Polymer Journal* **2021,** *147*, 110300-110308.

28. Liu, S.; Brunel, D.; Sun, K.; Zhang, Y.; Chen, H.; Xiao, P.; Dumur, F.; Lalevee, J., Novel photoinitiators based on benzophenone-triphenylamine hybrid structure for LED photopolymerization. *Macromolecular Rapid Communications* **2020,** *41* (23), e2000460.

29. Sun, K.; Xu, Y.; Dumur, F.; Morlet-Savary, F.; Chen, H.; Dietlin, C.; Graff, B.; Lalevée, J.; Xiao, P., In silico rational design by molecular modeling of new ketones as photoinitiators in three-component photoinitiating systems: Application in 3D printing. *Polymer Chemistry* **2020,** *11* (12), 2230-2242.

30. Graff, B.; Klee, J. E.; Fik, C.; Maier, M.; Fouassier, J. P.; Lalevée, J., Development of novel photoinitiators as substitutes of camphorquinone for the LED induced polymerization of methacrylates: A bis-silyl ketone. *Macromolecular Rapid Communications* **2017,** *38* (13).

31. Mau, A.; Le, T. H.; Dietlin, C.; Bui, T.-T.; Graff, B.; Dumur, F.; Goubard, F.; Lalevee, J., Donor–acceptor–donor structured thioxanthone derivatives as visible photoinitiators. *Polymer Chemistry* **2020,** *11* (45), 7221-7234.

32. Mau, A.; Dietlin, C.; Dumur, F.; Lalevée, J., Concomitant initiation of radical and cationic polymerisations using new copper complexes as photoinitiators: Synthesis and characterisation of acrylate/epoxy interpenetrated polymer networks. *European Polymer Journal* **2021,** *152*.

33. Chen, H.; Noirbent, G.; Liu, S.; Brunel, D.; Graff, B.; Gigmes, D.; Zhang, Y.; Sun, K.; Morlet-Savary, F.; Xiao, P.; Dumur, F.; Lalevée, J., Bis-chalcone derivatives derived from natural products as near-UV/visible light sensitive photoinitiators for 3D/4D printing. *Materials Chemistry Frontiers* **2021,** *5* (2), 901-916.

34. Chen, H.; Noirbent, G.; Sun, K.; Brunel, D.; Gigmes, D.; Morlet-Savary, F.; Zhang, Y.; Liu, S.; Xiao, P.; Dumur, F.; Lalevée, J., Photoinitiators derived from natural product scaffolds: mono-chalcones in three-component photoinitiating systems and their applications in 3D printing. *Polymer Chemistry* **2020,** *11* (28), 4647-4659.

35. Chen, H.; Noirbent, G.; Zhang, Y.; Brunel, D.; Gigmes, D.; Morlet-Savary, F.; Graff, B.; Xiao, P.; Dumur, F.; Lalevée, J., Novel D–π-A and A–π-D–π-A three-component photoinitiating systems based on carbazole/triphenylamino based chalcones and application in 3D and 4D printing. *Polymer Chemistry* **2020,** *11* (40), 6512-6528.

36. Chen, H.; Noirbent, G.; Zhang, Y.; Sun, K.; Liu, S.; Brunel, D.; Gigmes, D.; Graff, B.; Morlet-Savary, F.; Xiao, P.; Dumur, F.; Lalevée, J., Photopolymerization and 3D/4D applications using newly developed dyes: search around the natural chalcone scaffold in photoinitiating systems. *Dyes and Pigments* **2021,** *188*, 109213-109225.

37. Tehfe, M.-A.; Dumur, F.; Xiao, P.; Delgove, M.; Graff, B.; Fouassier, J.-P.; Gigmes, D.; Lalevée, J., Chalcone derivatives as highly versatile photoinitiators for radical, cationic, thiol–ene and IPN polymerization reactions upon exposure to visible light. *Polymer Chemistry* **2014,** *5* (2), 382-390.

38. Wang, X.; Jiang, M.; Zhou, Z.; Gou, J.; Hui, D., 3D printing of polymer matrix composites: A review and prospective. *Composites Part B: Engineering* **2017,** *110*, 442-458.

39. Xing, H.; Zou, B.; Lai, Q.; Huang, C.; Chen, Q.; Fu, X.; Shi, Z., Preparation and characterization of UV curable Al2O3 suspensions applying for stereolithography 3D printing ceramic

microcomponent. *Powder Technology* **2018,** *338*, 153-161.

40. Schwentenwein, M.; Homa, J., Additive manufacturing of dense alumina ceramics. *International Journal of Applied Ceramic Technology* **2015,** *12* (1), 1-7.

41. Song, S. Y.; Park, M. S.; Lee, D.; Lee, J. W.; Yun, J. S., Optimization and characterization of high-viscosity ZrO2 ceramic nanocomposite resins for supportless stereolithography. *Materials & Design* **2019,** *180*.

42. Zhang, Y.; Josien, L.; Salomon, J.-P.; Simon-Masseron, A.; Lalevée, J., Photopolymerization of zeolite/polymer-based composites: Toward 3D and 4D printing applications. *ACS Applied Polymer Materials* **2020,** *3* (1), 400-409.

43. Zhang, Y.; Liu, S.; Chen, H.; Josien, L.; Schrodj, G.; Simon-Masseron, A.; Lalevée, J., Development of a zeolite/polymer-based hydrogel composite through photopolymerization for 3D printing application. *Macromolecular Materials and Engineering* **2021**, 2100129-2100135.

44. Xu, Y.; Ding, Z.; Zhu, H.; Zhang, Y.; Knopf, S.; Xiao, P.; Lalevée, J., Preparation of iron filler-based photocomposites and application in 3D printing. *Macromolecular Materials and Engineering* **2020,** *306* (3), 2000720-2000725.

45. Kalsoom, U.; Peristyy, A.; Nesterenko, P. N.; Paull, B., A 3D printable diamond polymer composite: A novel material for fabrication of low cost thermally conducting devices. *RSC Advances* **2016,** *6* (44), 38140-38147.

46. Layani, M.; Wang, X.; Magdassi, S., Novel materials for 3D printing by photopolymerization. *Advanced Materials* **2018,** *30* (41), E1706344-E1706350.

47. Baerlocher, C.; McCusker, L. B.; Olson, D. H., *Atlas of zeolite framework types*. Elsevier: 2007.

48. Thakkar, H.; Eastman, S.; Hajari, A.; Rownaghi, A. A.; Knox, J. C.; Rezaei, F., 3D-printed zeolite monoliths for CO2 removal from enclosed environments. *ACS Applied Materials & Interfaces* **2016,** *8* (41), 27753-27761.

49. Thakkar, H.; Lawson, S.; Rownaghi, A. A.; Rezaei, F., Development of 3D-printed polymer-zeolite composite monoliths for gas separation. *Chemical Engineering Journal* **2018,** *348*, 109-116.

50. Thommes, M.; Kaneko, K.; Neimark, A. V.; Olivier, J. P.; Rodriguez-Reinoso, F.; Rouquerol, J.; Sing, K. S. W., Physisorption of gases, with special reference to the evaluation of surface area and pore size distribution (IUPAC Technical Report). *Pure and Applied Chemistry* **2015,** *87* (9-10),

1051-1069.

51. Zhang, W.; Xu, F.; Wang, Y.; Luo, M.; Wang, D., Facile control of zeolite NaA dispersion into xanthan gum–alginate binary biopolymer network in improving hybrid composites for adsorptive removal of Co2+ and Ni2+. *Chemical Engineering Journal* **2014,** *255*, 316-326.

52. Mittal, H.; Al Alili, A.; Alhassan, S. M., Adsorption Isotherm and Kinetics of Water Vapors on Novel Superporous Hydrogel Composites. *Microporous and Mesoporous Materials* **2020,** *299*.

53. Cursaru, B.; Radu, A.-L.; Perrin, F.-X.; Sarbu, A.; Teodorescu, M.; Gavrilă, A.-M.; Damian, C.-M.; Sandu, T.; Iordache, T.-V.; Zaharia, A., Poly(ethylene glycol) composite hydrogels with natural zeolite as filler for controlled delivery applications. *Macromolecular Research* **2019,** *28* (3), 211-220.

TOC graphic: (propose a TOC)